Chinese Journal of Electronics
vol. 33, no. 5, pp. 1234–1244, September 2024
https://doi.org/10.23919/cje.2023.00.064

RESEARCH ARTICLE

Wideband Millimeter Wave Antenna with Cavity Backed Slotted Patch and Magneto-Electric Dipole

Yang CHENG and Yuandan DONG

School of Electronic Science and Engineering, University of Electronic Science and Technology of China, Chengdu 611731, China

Corresponding author: Yuandan DONG, Email: ydong@uestc.edu.cn
Manuscript Received March 3, 2023; Accepted December 12, 2023

Abstract — This paper proposes a wideband cavity-backed slotted patch antenna, loaded with a magneto-electric (ME)-dipole and fed by a microstrip line, for millimeter wave (mm-Wave) applications. The coupled-feed cavity-backed slotted patch antenna is loaded with the ME-dipole. The slotted patch antenna serves as both a radiator and a ground for the ME-dipole. The combination of the ME-dipole antenna and the slotted patch antenna realizes a –10 dB impedance bandwidth covering over 22.86–44.35 GHz (63.9%). The pattern of the antenna element remains stable throughout this bandwidth. The proposed broadband antenna unit not only realizes single linearly polarized (LP) radiation but also can be designed for dual-LP radiation. The dual-polarized radiation can be achieved by changing the slot of the patch antenna to a crossed slot and altering the ME-dipole antenna to a dual-polarization form. A 2 × 2 dual-polarized array has been designed, fabricated, and tested. A novel dual-polarized feeding network is proposed. To achieve higher isolation, broadband in-phase feed and differential feed are adopted, respectively. A low-loss single to the differential structure is proposed for differential feeding. The simulated isolation of the array is higher than 40 dB. Measured results show that the dual-polarized 2 × 2 array has an overlapping bandwidth of 52.3% ($|S_{11}| < -10$ dB and $|S_{21}| < -30$ dB) with a peak gain of 14 dBi. The proposed antenna, featuring a wide overall bandwidth, low cost, and good radiation performance, is well suited for mm-Wave applications.

Keywords — Array antenna, Dual-polarized antenna, Feeding network, Magneto-electric dipole, Millimeter-wave (mm-Wave), Patch.

Citation — Yang CHENG and Yuandan DONG, "Wideband Millimeter Wave Antenna with Cavity Backed Slotted Patch and Magneto-Electric Dipole," *Chinese Journal of Electronics*, vol. 33, no. 5, pp. 1234–1244, 2024. doi: 10.23919/cje.2023.00.064.

I. Introduction

Millimeter wave (mm-Wave) communication has been garnering increased attention due to its wide frequency band and high transmission rate [1]–[4]. As illustrated in Figure 1, the mm-Wave frequency band has a broad array of potential applications and prospects, including 5G communication [5]–[7], satellite communication [8], and autonomous driving mm-Wave radar [9]–[11], etc. Despite the significant advantages of the mm-Wave frequency band, it also has notable drawbacks, including substantial transmission loss, limited base station coverage, and high cost. Given the factors of transmission loss (atmospheric attenuation window) and system cost (processing and testing cost), the Ka-band is currently widely used [1].

High-performance, low-cost mm-Wave antennas and arrays, being key components in communication systems, have been the focus of extensive research in recent years. Planar antennas based on printed circuit board (PCB) processing technology are more suitable for large-scale mm-Wave applications due to their potential for cost reduction and high integration. Various PCB-based transmission structures, such as substrate-integrated waveguides (SIW) [12]–[20], substrate-integrated coaxial lines (SICL) [21], printed ridge gap waveguides (PRGW) [22], and microstrip lines [23]–[30], have been implemented in mm-Wave antennas. While SIW and SICL exhibit lower loss, the single-mode transmission bandwidth of SIW restricts the working bandwidth of the feed network, and

Associate Editor: Prof. Yinghong WEN, Beijing Jiaotong University.

Figure 1 Schematic diagram of mm-Wave application scenarios.

the SICL's structure is more complex, making its design more challenging. Furthermore, implementing a dual-polarized feed network using PRGW or other structures [31]–[33] poses challenges.

Patch antennas and magneto-electric (ME)-dipole antennas are routinely employed as planar mm-Wave radiators. Typically, patch antennas have a narrow bandwidth. Common methods for bandwidth expansion include adding parasitic patches [19] and increasing the back cavity [13], [17], [18]. A wideband cavity-backed patch antenna, with a gain and impedance bandwidth overlap of better than 36%, was proposed in [13]. An air cavity enhances impedance matching, suppresses the surface wave, and directs energy toward the boresight direction. A 16 × 16 cavity-backed patch antenna array with SIW feed networks was demonstrated in [17], achieving a gain up to 30.1 dBi, a 3 dB gain bandwidth of 16.1%, an impedance bandwidth (VSWR < 2) of 15.3%, and symmetrical broadside radiation patterns. Despite their excellent performance, it is challenging for these planar mm-Wave patch antennas to cover the entire Ka-band bandwidth.

For a wider bandwidth, planar ME-dipole antennas are commonly used in the mm-Wave band. A mm-Wave 4 × 4 ME-dipole antenna array using a packaged microstrip line feed network was presented in [23]. This antenna element uses an L-probe feed method, and the array features an impedance bandwidth of more than 50% and minimal back radiation. Nonetheless, this feed method makes realizing dual-polarized radiation difficult. Reference [24] uses an L-shaped probe feed, similar to [23], to achieve wideband dual-polarized radiation, but the required LTCC (low temperature co-fired ceramic) process is high-cost and the antenna efficiency is low. The isolation of the array in [24] is small (>14 dB). A broadband (bandwidth around 44.6%) linearly polarized (LP) substrate-integrated ME-dipole with a low-profile microstrip feeding structure was proposed in [26]. An additional segment expands the bandwidth of the ME-dipole. However, this structure is challenging to use for dual-polarized radiation. A wideband dual-polarized ME-dipole was presented in [27], using two pairs of T-shaped probes to feed the ME-dipole. A 2 × 2 array was designed in [27], and the measured results show an impedance bandwidth of 50% with isolation of 17.6 dB. The isolation of the antenna element and array proposed in [27] is low, and as the feeding network is designed on the same layer, though it allows for a lower profile, it is challenging to scale up to a large array.

In summary, designing broadband, scalable planar mm-Wave array antennas capable of expandable dual-polarized radiation with high isolation is a key challenge in mm-Wave systems. To address this issue, this paper proposes a cavity-backed slotted patch antenna combined with an ME-dipole antenna for a broadband design. The slotted patch antenna serves both as a radiator and a ground for the ME-dipole. For verification purposes, we design and propose single LP elements, dual-LP elements, and arrays. The following contributions are made in this study:

1) A broadband planar single-LP antenna structure is proposed. By integrating an ME-dipole antenna with a slotted patch antenna, we achieve an impedance bandwidth of −10 dB, spanning from 22.86 GHz to 44.35 GHz (63.9%) and a peak gain of 9.9 dBi. The pattern of the antenna element remains stable across the entire operational band.

2) A dual-LP structure is then designed to suit different application scenarios. Simulated results reveal that the two polarization states each achieve an impedance bandwidth of 52.1% and 53.6%, respectively, with peak gains of 8.7 dBi and 9.2 dBi. The isolation surpasses 20 dB over the entire band.

3) A novel dual-polarized feed network is proposed to accommodate both wideband and high isolation. Leveraging this feed network, we designed, processed, and tested a 2 × 2 array. As per the measured results, an overlapping bandwidth of 52.3% (with $|S_{11}| < -10$ dB and $|S_{21}| < -30$ dB) and a peak gain of 14 dBi are achieved.

II. Single-LP Antenna

1. Configuration of single-LP antenna

Figure 2 displays the configuration of the proposed single-LP antenna element. Figure 2(a) presents an exploded view of the antenna. The cavity-backed slotted patch antenna is loaded with an ME-dipole and is energized by the microstrip line through slot coupling. The top view and a detailed view of the antenna are shown in Figures 2(b) and (c). The antenna comprises three substrates and a bonding layer, with the stacked structure shown in Figure 2(d). The material for the three substrate layers is F4BME220, which has a dielectric constant of 2.2 and a loss tangent of 0.001. The bonding layer uses Rogers 4450 with a thickness of 0.1 mm. The main reasons for using microstrip line feed are: 1) The microstrip feed network can achieve a wider impedance bandwidth; 2) The design is relatively simple; 3) The profile is low compared with other transmission lines such as SIW, SICL, and PRGW. The patch antenna and the E-dipole antenna are printed on the bottom layer and top layer of the Sub1, respectively. The cavity is implemented on Sub2. Sub3 and Sub2 are bonded together through a bonding layer, with the microstrip line positioned at the bottom layer of Sub3. Sub3 and the bond-

ing layer form a combined substrate, and its equivalent dielectric constant can be calculated using the method presented in [26].

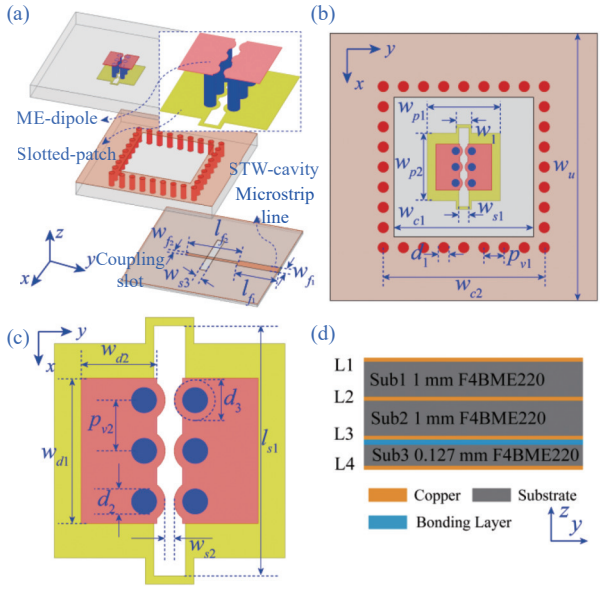

Figure 2 Configuration of the proposed single-LP element. (a) Exploded view; (b) Top view; (c) Detailed view of the slotted patch loaded ME-dipole; (d) Layer structure. (w_{f1}=0.6, w_{f2}=0.213, l_{f1}=3.088, l_{f2}=3.82, w_{p1}=2.73, w_{p2}=2.54, w_1=0.57, w_{c1}=5.23, w_{c2}=6.03, w_u=10, d_1=0.4, d_2=0.3, d_3=0.5, p_{v1}=0.75, p_{v2}=0.6, w_{s1}=0.37, w_{s2}=0.1, w_{s3}=0.5, l_{s1}=2.96, w_{d1}=1.72, w_{d2}=0.89, Unit: mm)

2. Operating principle

The proposed antenna element has a very wide impedance bandwidth, mainly due to the combination of a cavity-backed slotted patch and an ME-dipole antenna. The primary design concept and process are illustrated in Figure 3. Note that Sub1 from Figure 2 is not shown in Figure 3 for clarity. For the proposed antenna, a slot is etched in the middle of the cavity-backed patch to excite the loaded ME-dipole antenna above. The patch antenna functions both as a radiator and as a ground for the ME-dipole antenna. When the antenna operates in the low-frequency band, the proposed antenna can be considered a thicker patch antenna, with the patch mode being the primary radiation mode. At high frequencies, the ME-dipole antenna is the main radiator. Both patch antennas and ME-dipole antennas are widely utilized in

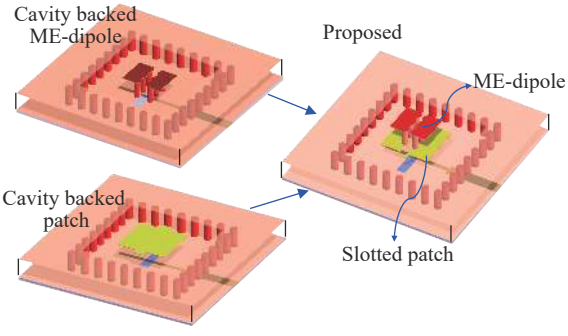

Figure 3 Design idea and process of the proposed antenna.

mm-Wave systems. The combination of these two antennas is also relatively straightforward and only requires low-cost PCB processing technology. A comparison of the proposed antenna with a cavity-only, cavity-backed ME-dipole, and cavity-backed patch antenna in terms of $|S_{11}|$ is shown in Figure 4. The simulation model in Figure 4 can refer to Figure 3, and the structural parameters are identical to the proposed antenna. It can be observed that, for the patch only, or when the cavity is combined with a patch or an ME-dipole, there are fewer resonance modes, and achieving ultra-wideband matching is challenging.

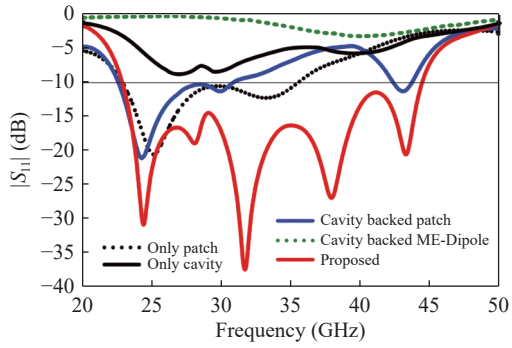

Figure 4 Comparison of the proposed antenna with cavity-only, cavity backed ME-dipole and cavity backed patch antenna in terms of $|S_{11}|$.

To elucidate the operational principle of the proposed antenna, we present the electric field vector distribution diagrams of the conventional cavity-backed patch antenna, the cavity-backed patch antenna loaded with an ME-dipole antenna and the proposed antenna structure at 26 GHz and 36 GHz in Figure 5. As evident from Figures 5(a) and (b), the operational modes of the coupled cavity-backed patch antennas at both 26 GHz and 36 GHz are TM_{10} modes (In the notation TM_{mn}, "m" indicates the number of half-wave variations in the electric field along the length of the patch, and "n" indicates the number of half-wave variations along the width of the patch.).

The structure in Figures 5(c) and (d) demonstrates the loading of an ME-dipole antenna onto the patch antenna depicted in Figures 5(a) and (b). One can observe that the ME-dipole antenna remains unexcited, and the primary operational mode is still the TM_{10} mode of the patch antenna. It can be considered that the structure in Figures 5(c) and (d) represents a thicker patch antenna.

Building on Figures 5(c) and (d), a slot is etched in the middle of the patch. It should be noted that this slot should not completely divide the patch antenna into two halves, as it would disable the support for the primary mode of the patch antenna. This slot excites the ME-dipole antenna loaded on the patch antenna. Figures 5(e) and (f) reveal that both the patch mode and the ME-dipole mode are excited in the proposed antenna structure.

To better elucidate the roles of the cavity-backed patch and ME-dipole in the overall structure, several key

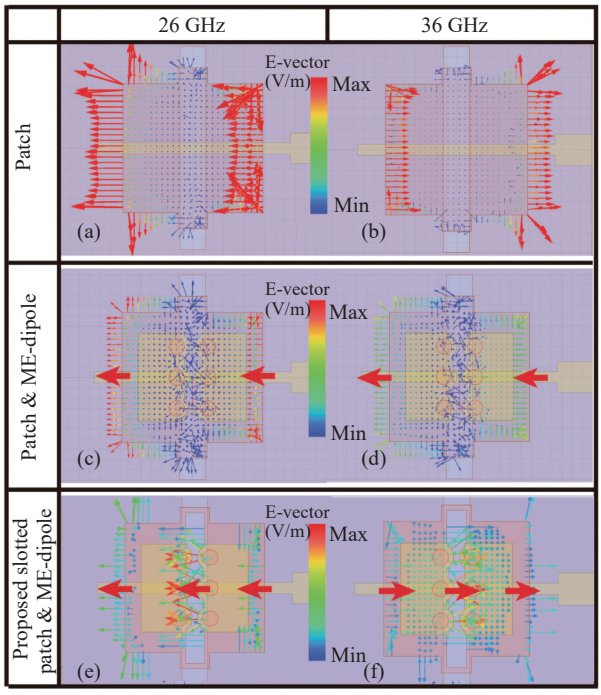

Figure 5 Simulated E-vector of the different antenna. Patch antenna at (a) 26 GHz and (b) 36 GHz. Patch loaded ME-dipole antenna at (c) 26 GHz and (d) 36 GHz. Proposed slotted patch loaded ME-dipole antenna at (e) 26 GHz and (f) 36 GHz.

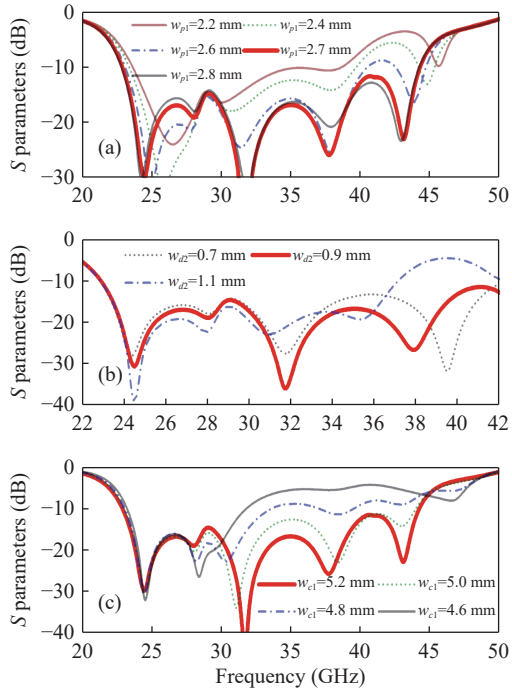

Figure 6 Simulated $|S_{11}|$ parameters with different values of w_{p1}, w_{d2} and w_{c1}. (a) $|S_{11}|$ of different w_{p1}; (b) $|S_{11}|$ of different w_{d2}; (c) $|S_{11}|$ of different w_{c1}.

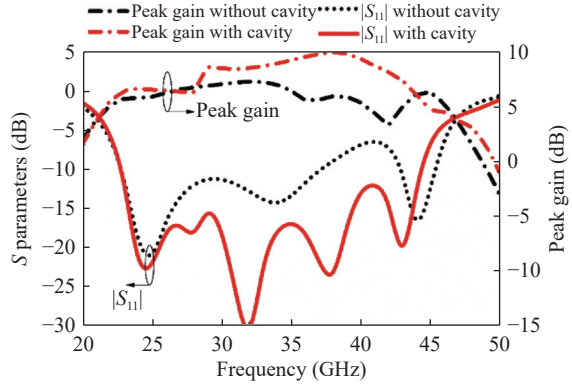

Figure 7 Simulated effect of cavity on the S parameters and peak gain.

parametric studies are conducted. Figure 6 illustrates the effects of different values of w_{p1}, w_{d2}, and w_{c1} on the $|S_{11}|$ curve. According to the primary theory of the patch antenna, the length of w_{p1} controls the resonance frequency of the patch antenna, while w_{d2} controls the resonance frequency of the E-dipole in the ME-dipole. Figures 6(a) and (b) demonstrate the effects of these two parameters on the $|S_{11}|$. Given the large dimensions of the patch antenna, it primarily contributes to the resonance mode in the lower frequency band in this study; thus, a longer antenna length corresponds to a lower resonant frequency near 25 GHz. In addition, the slotted patch antenna proposed in this study also acts as the ground for the ME-dipole antenna. Alterations in the ground size would impact the resonance frequency and impedance matching of the ME-dipole antenna, subsequently affecting the high-frequency matching and resonant frequency. The shorter the w_{p1} and w_{d2}, the more the corresponding resonance points shift to the high-frequency band. The influence of the size of the ME-dipole on the resonance point of the patch is not evident because the size changes of the ME-dipole do not directly affect the w_{p1} of the patch antenna (Figure 6(b)). As illustrated from Figure 6(c), the size of the cavity will significantly impact the matching of the antenna; for a detailed discussion, refer to [13]. Figure 7 also illustrates the simulated effect of the cavity on the $|S_{11}|$ and peak gain. The cavity can improve the gain of the antenna, reduce the surface wave of the antenna on the substrate, and improve the matching of the antenna.

3. Simulated results of single-LP antenna

Figure 8 illustrates the simulated $|S_{11}|$, peak gain, and efficiency of the proposed single-LP antenna element. It can achieve a wide −10 dB impedance bandwidth of 22.86–44.35 GHz (63.9%). The peak gain of the antenna is higher than 6 dBi, and the efficiency exceeds 80% over the entire impedance bandwidth. The curve shows that the peak gain sharply increases (about 2 dB) around 28–29 GHz, mainly due to the influence of the cavity and substrate size. Refer to the peak gain curve in Figure 7. The gain curve is smoother at the low-frequency band in the absence of a cavity. Despite fluctuations in gain, the radiation pattern of the antenna does not deteriorate, only slight changes in the beamwidth occur, which do not impact the overall performance. Figure 9 shows the radiation patterns at 26 GHz and 36 GHz, with a wider beamwidth for the radiation patterns at 26 GHz. To better

showcase the advantages of our proposed antenna structure, Table 1 provides a performance comparison with the broadband planar mm-Wave antenna. Compared to the cavity-backed patch antenna [13] and conventional ME-dipole antenna [23], the proposed structure exhibits obvious advantages in bandwidth. The antenna has a 3 dB gain bandwidth of approximately 28.9%, and the gain fluctuates by less than 3.6 dB within the entire working bandwidth (63.9%). However, the antenna pattern remains stable throughout the entire bandwidth, and fluctuations in gain do not affect the overall performance of the antenna.

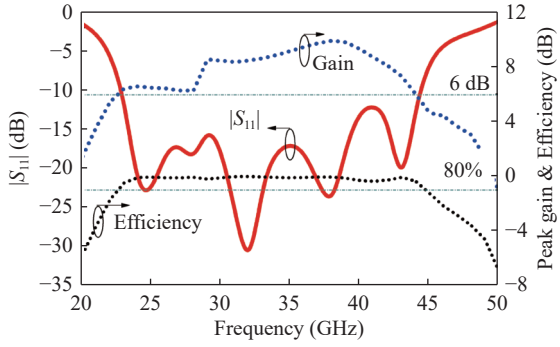

Figure 8 Simulated S parameters, peak gain and efficiency of the proposed single-LP element.

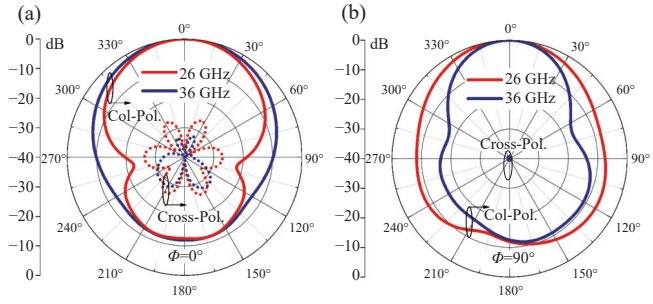

Figure 9 Simulated radiation patterns of proposed single-LP element at 26 GHz and 36 GHz. (a) Φ=0°; (b) Φ=90°.

Table 1 Performance comparisons of single-polarized antenna

Ref.	Frequency (GHz)	−10 dB IMB[1]	Peak gain (dBi)	3 dB gain bandwidth	Dual-pol. extended
[13]	64.7	36.2%	8.2	>36.2%	Yes
[17]	60.45	10.7%	N.A.	N.A.	Yes
[21]	32	50%	6.42	N.A.	No
[23]	32.15	54.4%	8.3	54.4%	Yes
[26]	29.14	43.5%	8.98	43.5%	No
Prop. Ant.	**33.6**	**63.9%**	**9.9**	**28.9% (3 dB) 63.9% (3.6 dB)**	**Yes**

Note: [1]IMB: impedance bandwidth. N.A.: not applicable.

III. Dual-Polarized Element

In addition to wide operating bandwidth, polarization diversity is another effective means to enhance the performance of mm-Wave communication systems [2], [34]. Consequently, dual-polarized antennas and arrays are now in widespread use. The patch antenna and ME-dipole antenna can be easily extended to a dual-polarized structure. Therefore, the proposed antenna structure can also be effortlessly extended into a dual-polarized radiator. This section will present the structure and simulated performance of the dual-polarized wideband element.

1. Configurations of dual-polarized element

Figure 10 shows the configurations of the proposed dual-polarized element based on the structure in Figure 2. The antenna structure is changed to a symmetrical structure and the slots are replaced with crossed slots. The PCB laminated structure of the dual-polarized element is depicted in Figure 11. The feed structure used for the dual-polarized element has been extensively utilized and validated, as referenced in [28]. The laminated structure is almost the same as that a single-polarized antenna, except that there is a feeding network (Pol.2 feed) on the top layer of Sub3. The bonding layer uses Rogers 4450 with a thickness of 0.1 mm. The two polarized feed structures are placed orthogonally to achieve high isolation. The feed line of Pol.2 is covered by Sub3 and the bonding layer, and the distance between Pol.2 and the ground is small, so the line width of Pol.2 is thin, which may cause large relative errors in actual processing.

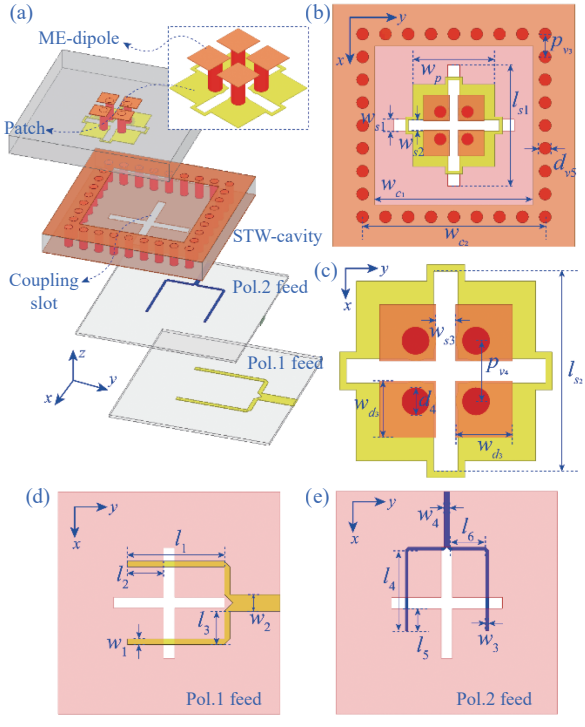

Figure 10 Configurations of proposed dual-polarized element. (a) Exploded view; (b) Top view; (c) Detailed view of patch loaded ME-dipole; (d) Pol.1 feed structure; (e) Pol.2 feed structure. (w_p=2.7, w_{s1}=0.4, w_{s2}=0.37, w_{s3}=0.3, l_{s1}=3.99, l_{s2}=3, w_{c1}=5.23, w_{c2}=6.03, p_{v3}=0.75, p_{v4}=0.9, w_{d3}=0.85, d_{v4}=0.4, d_{v5}=0.4, l_1=3.5, l_2=1.3, l_3=1.1, l_4=2.9, l_5=0.8, l_6=1.3, w_1=0.2, w_2=0.6, w_3=0.1, w_4=0.2. Unit: mm).

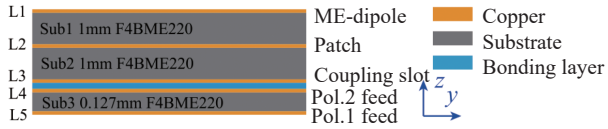

Figure 11 PCB laminated structure of dual-polarized element.

2. Simulated results of dual-polarized element

Figure 12 presents the simulated S parameters and peak gain of the proposed dual-polarized antenna element. Wide −10 dB impedance bandwidths of 24–40.93 GHz (52.1%) and 24.2–41.95 GHz (53.6%) are realized for the two polarization states, respectively. The peak gain of both polarizations exceeds 5.5 dBi over the entire impedance bandwidth. Port isolation is a crucial index for the dual-polarized antenna. The isolation of the proposed dual-polarized element is higher than 27 dB across the entire working bandwidth. Figure 13 shows the simulated radiation patterns of dual-polarized elements at 26 GHz and 36 GHz. The front-back ratio of the antenna exceeds 12 dB, the cross-polarization isolation surpasses 20 dB, and the overall pattern is relatively stable. Table 2 shows the performance comparison with the dual-polarized planar mm-Wave antenna element proposed in previous research work.

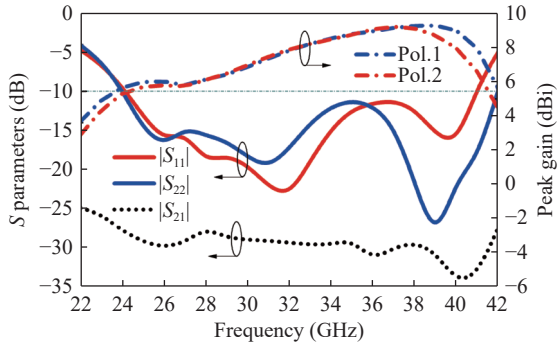

Figure 12 Simulated S parameters and peak gain of the proposed dual-polarized element.

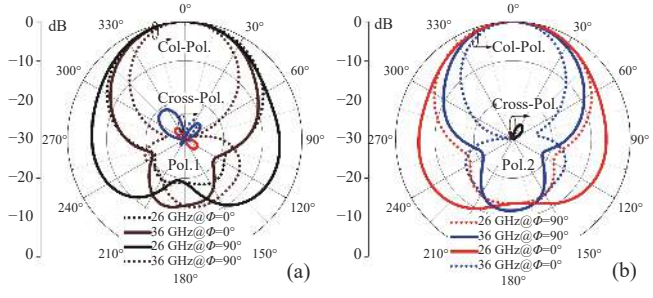

Figure 13 Simulated radiation patterns of dual-polarized element at 26 GHz and 36 GHz for (a) Pol.1 and (b) Pol.2.

IV. Dual-Polarized Array

1. Configurations of dual-polarized array

Figure 14 presents the configurations of the proposed 2 × 2 dual-polarized array. The exploded view of the array is shown in Figure 15. Due to the dual-polarized operation, the structure of the array is relatively more complex, and the design of the feed network is one of the main challenges. The array primarily consists of three layers of substrate, one layer of the bonding layer, and a metal cavity. The detailed laminated structure can be seen in Figure 16. Similar to the dual-polarized element, the three substrate layers are F4BME220, and the bonding layer is Rogers 4450 with a thickness of 0.1 mm. The purpose of the metal cavity is to increase the array gain. Two layers of feed networks are printed on the top layer (L2) and the bottom layer (L1) of Sub3, respectively. The feed network of Pol.1 is transmitted to the bot-

Table 2 Performance comparisons of dual-polarized antennas

Ref.	Frequency (GHz)	−10 dB IMB#1	Peak gain (dBi)	3 dB gain bandwidth	Isolation (dB)
[22]	30	23.4%	10.5	23.4%	20
[24]	33.65	42.5%	6.9	42.5%	24
[25]	28	5.7%	7.2	5.7%	>26.5
[27]	32	50%	9.3/9.4	N.A.	17.8
Prop. Ant.	**32.46 33**	**52.1% 53.6%**	**8.7/9.2**	**33.5% (3 dB) >50% (3.5 dB)**	**>27**

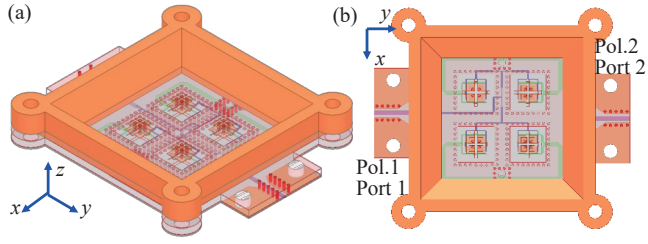

Figure 14 Configurations of proposed 2 × 2 dual-polarized array. (a) 3D view; (b) Top view.

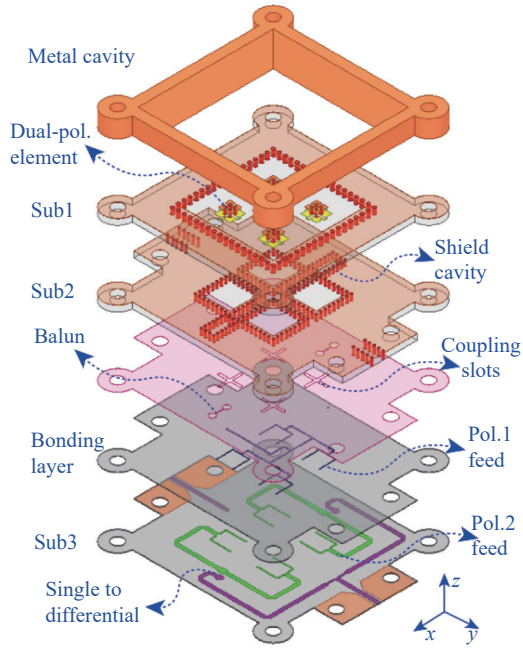

Figure 15 Exploded view of the 2 × 2 dual-polarized array.

tom layer of Sub3 through the metal via for testing. Sub2 and Sub3 are secured by a bonding layer. The top layer (L6) of Sub1 is an ME-dipole and the bottom layer (L5) is a patch antenna. The SIW cavity is realized on Sub2. The bottom layer of Sub1 (L5) overlaps with the top layer of Sub2 (L4). Finally, all structures are fixed with nylon screws in the positioning hole. The detailed structure of the two polarized feed networks is shown in Figure 17. Pol.1 uses a traditional in-phase feed network. To improve isolation, Pol.2 adopts two high-efficiency baluns to realize differential feeding.

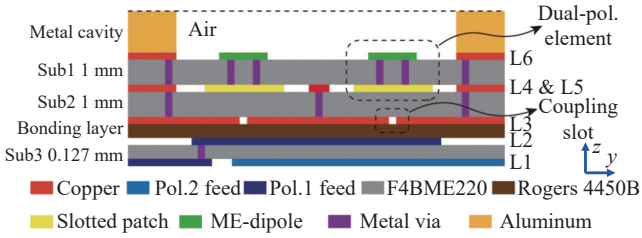

Figure 16 PCB laminated structure of the dual-polarized array.

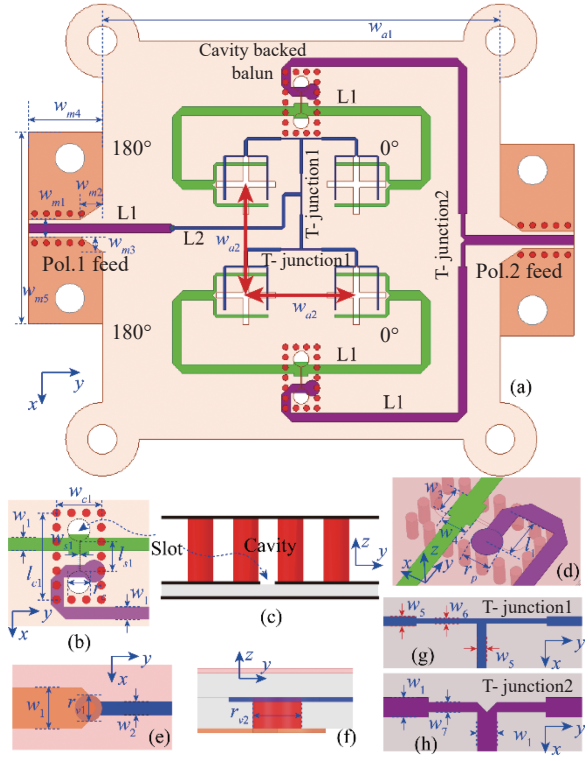

Figure 17 Configurations of dual-polarized feed network of proposed 2×2 array. (a) Top view; (b) Top view of balun; (c) Side view of balun in (b); (d) 3D view of Balun; (e) The transformation structure between the L1 and the L2 of the Pol.1 feed network; (f) Side view of (e); (g) and (h) Two types T-junctions. (w_{a1}=27, w_{a2}=7.5, w_{m1}=1.2, w_{m2}=1.5, w_{m3}=1, w_{m4}=5, w_{m5}=13, w_1=0.6, w_2=0.2, w_3=0.968, w_4=0.967, w_5=0.2, w_6=0.1, w_7=0.3, l_{s1}=1.44, w_{s1}=0.1, l_{c1}=4.14, w_{c1}=2.14, l_1=1.4, r_{v1}=0.4, r_{v2}=0.2, r_p=1, r_c=1. Unit: mm).

2. High isolation dual-polarized feed network

This subsection will introduce the main principles of the proposed high-isolation dual-polarized feed network. Figure 18 illustrates the electric field vector distribution at the balun when two ports are excited. It is evident that when port 2 is excited, the energy achieves a single terminal to differential conversion through the balun; when port 1 is excited, a differential signal cannot form at the balun, so it cannot be transmitted to port 2. Taking the excitation of port 1 as an example, Figure 19 shows the phase distribution during signal transmission. The feed network of Pol.1 will couple energy to the feed network of Pol.2, but it is the in-phase signal at the Balun, so it cannot be converted into a single-ended signal for transmission to port 2. Figure 20 displays the simulated E-field distribution when port 1 and port 2 are

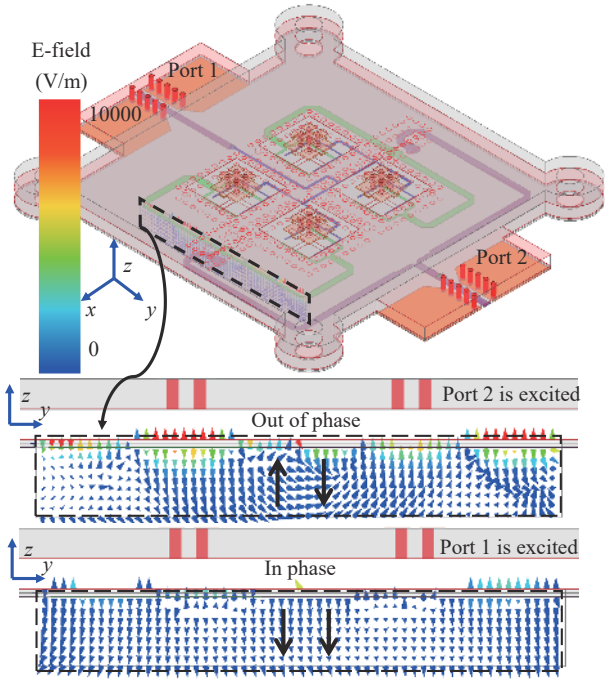

Figure 18 Electric field vector distribution of the balun when two ports are excited separately.

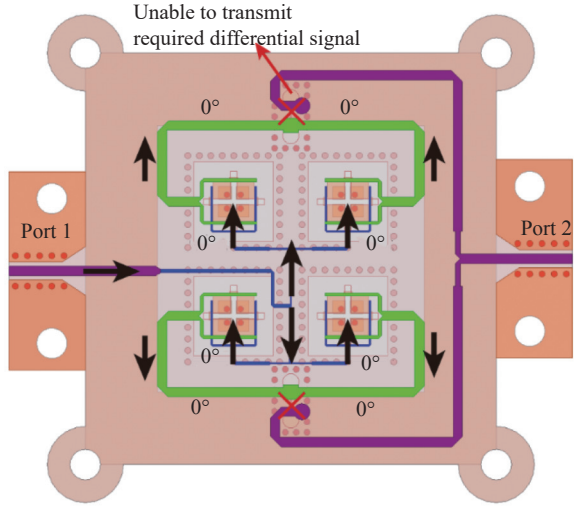

Figure 19 Phase distribution of feed line when port 1 is excited, where the field cannot be coupled to port 2 due to phase isolation.

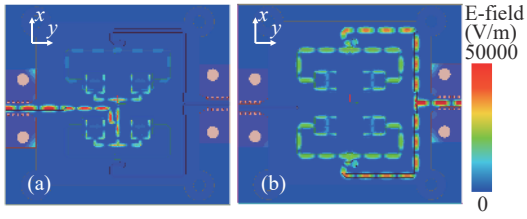

Figure 20 Simulated E-field distribution when (a) Port 1 and (b) Port 2 are excited, respectively.

excited, respectively. The isolation of the two ports is high, and the energy of one port is rarely transmitted to the other port during excitation.

For the proposed dual-polarized feed network, a low-loss wideband microstrip line balun is required for Pol.2. Wideband microstrip balun has been extensively studied [35]–[37], and is commonly used to convert single-ended signals to differential signals through a slot [35]. In the mm-Wave band, microstrip balun generally has an open structure and a large radiation loss. Therefore, according to our actual structure, we added a cavity to the slot to reduce the radiation loss. Figure 21 shows the structure and E-field distribution of the balun with and without the cavity. The cavity can block major radiation loss. Figure 22 showcases the influence of the cavity on the performance of the balun. The transmission loss can be reduced by more than 0.5 dB (Figure 22(a)) after the addition of the cavity, and the transmission phase is basically unaffected (Figure 22(b)).

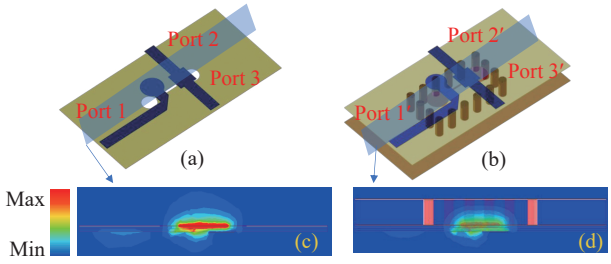

Figure 21 3D view of the balun and simulated E-field distribution (@30 GHz). (a) Balun without cavity; (b) Balun with the cavity; (c) E-Field in (a); (d) E-field in (b).

3. Simulated and measured results

Figure 23 shows a photograph of the proposed 2 × 2 dual-polarized array. Figure 24 illustrates the simulated and measured $|S_{11}|$ and $|S_{22}|$ of the dual-polarized array. Measured results show that a −10 dB impedance bandwidth of 53.4% (23.4–40 GHz) is realized for the two polarizations. Due to the frequency limitation of the test equipment, the actual test was only made to 40 GHz, while the simulated impedance bandwidth could cover 23.4–41.7 GHz (56%) and 24.73–40.66 GHz (52%) for two polarizations, respectively. Figure 25 displays the simulated and measured isolation. The measured isolation is higher than 30 dB in the operating band. Figure 26 shows the simulated and measured peak gain and simulated efficiency. Measured results show that a 3 dB gain

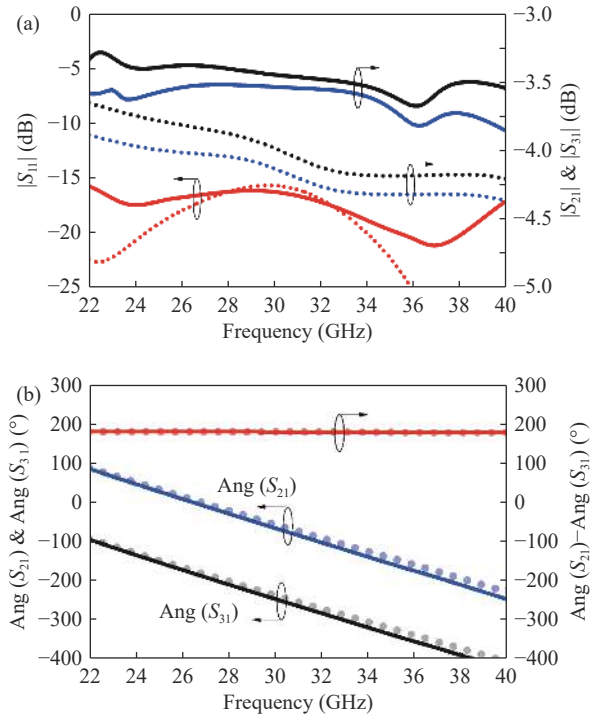

Figure 22 Effect of cavity on performance of balun. (a) Amplitude and (b) phase of the S parameters. (Solid line: with cavity. Dotted line: without cavity).

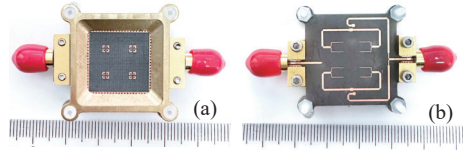

Figure 23 The fabricated prototype of the dual-polarized antenna array. (a) Top view; (b) Bottom view.

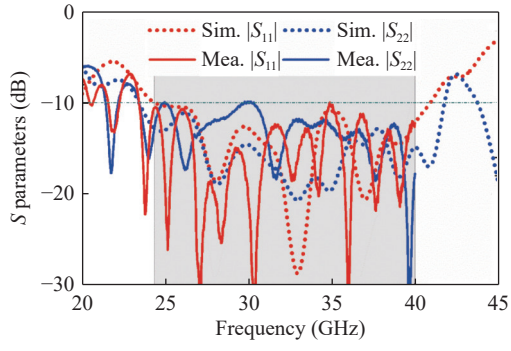

Figure 24 Simulated and measured $|S_{11}|$ and $|S_{22}|$ of proposed 2 × 2 dual-polarized array.

bandwidth of 26.5–40 GHz with a peak gain of 14 dBi is realized. The simulated 3 dB gain bandwidth can cover 24–41.8 GHz. Because the feed network of the dual-polarized array is more complex, the transmission loss is larger than that of the single-polarized array, and the simulated efficiency of the array is higher than 64% in the operating band. Although the tested frequency band does not fully cover the bandwidth of the array, it can still demonstrate the proposed antenna performance.

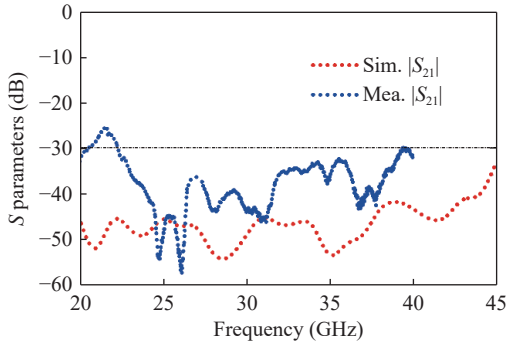

Figure 25 Simulated and measured isolation of proposed dual-polarized array.

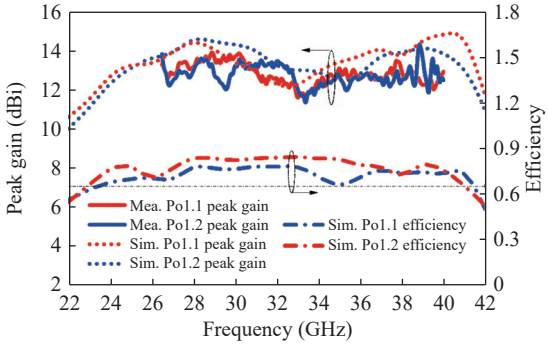

Figure 26 Simulated and measured peak gain and simulated efficiency.

Figure 27 depicts the simulated and measured radiation patterns of the array. The radiation patterns of the two polarizations of the array remain stable in the whole working band. The slight discrepancy is mainly due to machining and testing errors.

4. Comparison and discussion

To better describe the advantages of the antenna array proposed in this paper, Table 3 shows the performance comparison between single-polarized and dual-polarized planar array antennas. The common transmission line structure of the feed network mainly includes SIW, SICL, PRGW and microstrip lines. Although the transmission loss of the SIW has advantages in the millimeter wave band, it is difficult for the SIW feed network to achieve broadband design (generally no more than 35%), so it is difficult for antenna arrays based on SIW to achieve broadband radiation. The array based on SICL [21] and microstrip line [23], [24], [26], [27] can achieve more than 50% impedance bandwidth, but because of the relatively complex transmission line structure, it is difficult to realize dual polarized radiation. LTCC process can be used to achieve similar dual-polarization expansion [24], but the processing cost is high and the loss is large. In addition, the isolation between the two polarized ports is also relatively low (>14 dB). The single-polarized array proposed in [26] has wide impedance bandwidth and gain bandwidth. Our proposed structure has a wider impedance bandwidth. In conclusion, our proposed single-polarized and dual-polarized units and dual-polarized array have advantages in terms of bandwidth, isolation and processing cost.

V. Conclusion

This paper proposes a novel broadband antenna

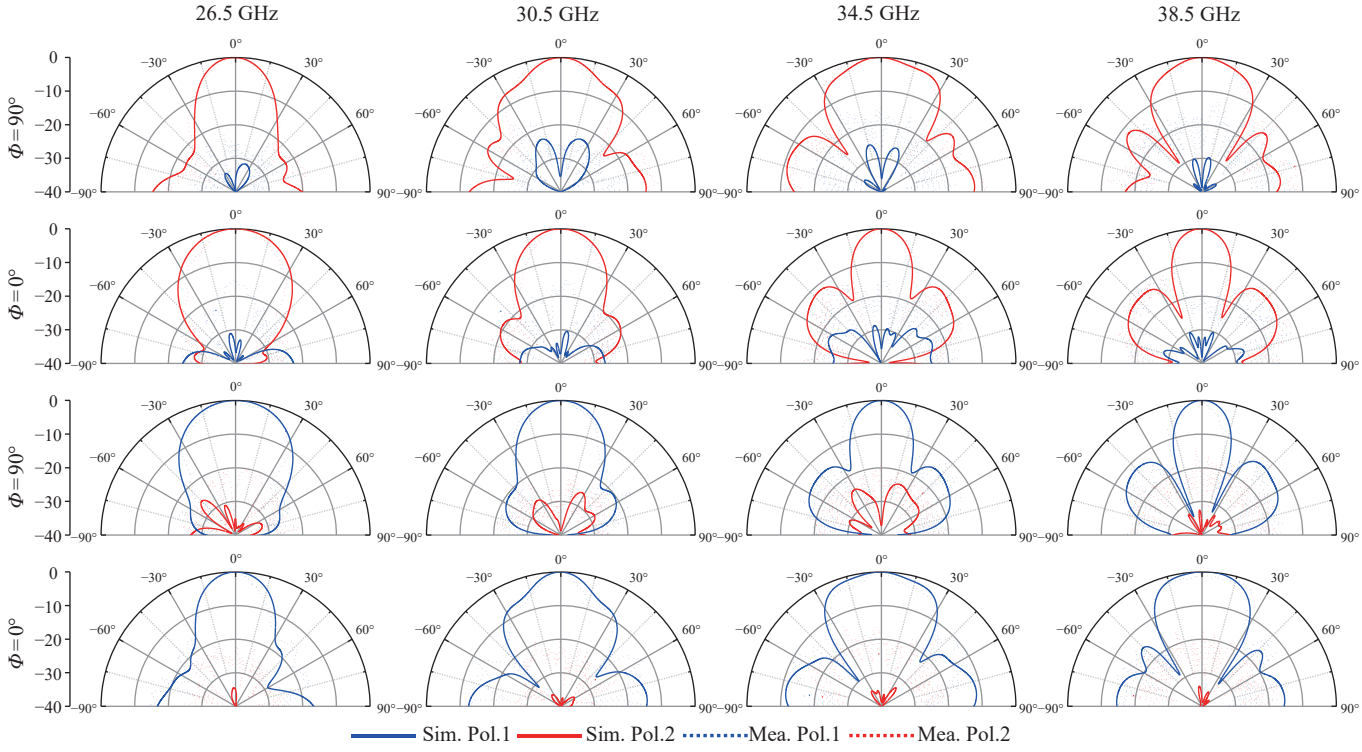

Figure 27 Simulated and measured radiation patterns. (Pol.1: Port 1 is excited. Pol.2: Port 2 is excited. See Figure 14).

Table 3 Comparisons between the proposed array and others

Ref.	Center frequency (GHz)	Polarization	Impedance bandwidth (−10 dB)	No. of elements	Peak gain (dBi)	3-dB gain bandwidth	Isolation (dB)	Feed line & Processing technology	Size ($\times\lambda_0^2$)#2
[14]	28	Single LP#1	8.5%	4×4	19.1	N.A.	N.A.	SIW / PCB	N.A.
[16]	27.75	Single LP	17.7%	4×4	16.4	N.A.	N.A.	SIW / PCB	1.85×1.85
[17]	60	Single LP	15.3%	16×16	30.1	16.1%	N.A.	SIW / PCB	12.16×12.16
[18]	60	Single LP	>18.2%	4×4	21.4	>18.2%	N.A.	SIW / PCB	6×6
[20]	39.5	Dual-LP	14.6%	8×8	25.8	14.6%	45	SIW / PCB	7.59×7.59
[21]	32	Single LP	50%	1×8	13.1	N.A.	N.A.	SICL / PCB	N.A.
[22]	30	Dual-LP	23.4%	1	10.5	N.A.	20	PRGW / PCB	1.2×1.2
[23]	32	Single LP	51.5%	4×4	20.3	43.8%	N.A.	PMS#3 / PCB	3.2×3.2
[24]	33	Dual-LP	45%	4×4	16.1	>39.4%	>14	MS#4 / LTCC	N.A.
[25]	28	Dual-LP	6%	2×8	16.7	N.A.	>20	MS / PCB	N.A.
[26]	28.32	Single LP	44.6%	4×4	19.18	>47.67	N.A.	MS / PCB	2.83×2.83
[27]	32	Dual-LP	>50%	2×2	14.8	40%	17.6	MS / PCB	N.A.
[30]	13.8	Dual-LP	26.37% 27.77%	2×2	N.A.	N.A.	32	QSIW / PCB	N.A.
Proposed array	**31.7**	**Dual-LP**	**>52.3%**	**2×2**	**14**	**>40.6% 52%&56%(Sim.)**	**>30**	**MS / PCB**	**2.87×2.87**

Note: #1Single linear polarization. #2λ_0 free space wavelength at center frequency. #3Packaged microstrip line. #4Microstrip line.

structure, demonstrating that the slotted patch antenna and the magneto-electric (ME) dipole antenna can be integrated to achieve a larger bandwidth. During this process, to address the issues of narrow bandwidth and low isolation in dual-polarized array feed networks, we propose a novel dual-polarized feed network topology. This allows for the realization of a low-cost, broadband, high-isolation feed network on a two-layer substrate. The proposed antenna has a simple working principle and excellent radiation performance and has obvious advantages in bandwidth, isolation and processing cost, which is very suitable for mm-Wave applications.

References

[1] D. X. Liu, W. B. Hong, T. S. Rappaport, *et al.*, "What will 5G antennas and propagation be?," *IEEE Transactions on Antennas and Propagation*, vol. 65, no. 12, pp. 6205–6212, 2017.

[2] T. S. Rappaport, Y. C. Xing, G. R. MacCartney, *et al.*, "Overview of millimeter wave communications for fifth-generation (5G) wireless networks—with a focus on propagation models," *IEEE Transactions on Antennas and Propagation*, vol. 65, no. 12, pp. 6213–6230, 2017.

[3] W. Hong, Z. H. Jiang, C. Yu, *et al.*, "Multibeam antenna technologies for 5G wireless communications," *IEEE Transactions on Antennas and Propagation*, vol. 65, no. 12, pp. 6231–6249, 2017.

[4] V. Va, T. Shimizu, G. Bansal, *et al.*, *Millimeter Wave Vehicular Communications: A Survey*. Now Foundations and Trends, Boston, MA, USA, 2016.

[5] M. C. Tang, T. Shi, and R. W. Ziolkowski, "A study of 28 GHz, planar, multilayered, electrically small, broadside radiating, Huygens source antennas," *IEEE Transactions on Antennas and Propagation*, vol. 65, no. 12, pp. 6345–6354, 2017.

[6] S. S. Li, T. Y. Chi, Y. J. Wang, *et al.*, "A millimeter-wave dual-feed square loop antenna for 5G communications," *IEEE Transactions on Antennas and Propagation*, vol. 65, no. 12, pp. 6317–6328, 2017.

[7] K. M. Mak, K. K. So, H. W. Lai, *et al.*, "A magnetoelectric dipole leaky-wave antenna for millimeter-wave application," *IEEE Transactions on Antennas and Propagation*, vol. 65, no. 12, pp. 6395–6402, 2017.

[8] Q. Luo, S. Gao, C. Zhang, *et al.*, "Design and analysis of a reflectarray using slot antenna elements for Ka-band SatCom," *IEEE Transactions on Antennas and Propagation*, vol. 63, no. 4, pp. 1365–1374, 2015.

[9] J. Hasch, E. Topak, R. Schnabel, *et al.*, "Millimeter-wave technology for automotive radar sensors in the 77 GHz frequency band," *IEEE Transactions on Microwave Theory and Techniques*, vol. 60, no. 3, pp. 845–860, 2012.

[10] B. Schoenlinner, X. D. Wu, J. P. Ebling, *et al.*, "Wide-scan spherical-lens antennas for automotive radars," *IEEE Transactions on Microwave Theory and Techniques*, vol. 50, no. 9, pp. 2166–2175, 2002.

[11] H. Abedi and G. Shaker, "Low-cost 3D printed dielectric hyperbolic lens antenna for beam focusing and steering of a 79 GHz MIMO radar," in *Proceedings of 2020 IEEE International Symposium on Antennas and Propagation and North American Radio Science Meeting*, Montreal, QC, Canada, pp. 1543–1544, 2020.

[12] W. M. Abdel-Wahab and S. Safavi-Naeini, "Wide-bandwidth 60-GHz aperture-coupled microstrip patch antennas (MPAs) fed by substrate integrated waveguide (SIW)," *IEEE Antennas and Wireless Propagation Letters*, vol. 10, pp. 1003–1005, 2011.

[13] I. M. Mohamed and A. R. Sebak, "60 GHz 2-D scanning multibeam cavity-backed patch array fed by compact SIW beamforming network for 5G applications," *IEEE Transactions on Antennas and Propagation*, vol. 67, no. 4, pp. 2320–2331, 2019.

[14] H. Y. Jin, W. Q. Che, K. S. Chin, *et al.*, "Millimeter-wave TE_{20}-mode SIW dual-slot-fed patch antenna array with a compact differential feeding network," *IEEE Transactions on Antennas and Propagation*, vol. 66, no. 1, pp. 456–461, 2018.

[15] G. H. Sun and H. Wong, "Circularly polarized elliptical cavity-backed patch antenna array for millimeter-wave applications," *IEEE Transactions on Antennas and Propagation*, vol. 70, no. 11, pp. 10512–10519, 2022.

[16] J. Xu, W. Hong, Z. H. Jiang, *et al.*, "Wideband, low-profile

patch array antenna with corporate stacked microstrip and substrate integrated waveguide feeding structure," *IEEE Transactions on Antennas and Propagation*, vol. 67, no. 2, pp. 1368–1373, 2019.
[17] Y. J. Li and K. M. Luk, "60-GHz substrate integrated waveguide fed cavity-backed aperture-coupled microstrip patch antenna arrays," *IEEE Transactions on Antennas and Propagation*, vol. 63, no. 3, pp. 1075–1085, 2015.
[18] J. F. Zhu, C. H. Chu, L. Deng, *et al.*, "Mm-wave high gain cavity-backed aperture-coupled patch antenna array," *IEEE Access*, vol. 6, pp. 44050–44058, 2018.
[19] H. F. Xu, J. Y. Zhou, K. Zhou, *et al.*, "Planar wideband circularly polarized cavity-backed stacked patch antenna array for millimeter-wave applications," *IEEE Transactions on Antennas and Propagation*, vol. 66, no. 10, pp. 5170–5179, 2018.
[20] B. T. Feng, Y. T. Tu, J. L. Chen, *et al.*, "Dual linearly-polarized antenna array with high gain and high isolation for 5G millimeter-wave applications," *IEEE Access*, vol. 8, pp. 82471–82480, 2020.
[21] F. F. Fan, Q. L. Chen, Y. X. Xu, *et al.*, "A wideband compact printed dipole antenna array with SICL feeding network for 5G application," *IEEE Antennas and Wireless Propagation Letters*, vol. 22, no. 2, pp. 283–287, 2023.
[22] M. M. M. Ali, I. Afifi, and A. R. Sebak, "A dual-polarized magneto-electric dipole antenna based on printed ridge gap waveguide technology," *IEEE Transactions on Antennas and Propagation*, vol. 68, no. 11, pp. 7589–7594, 2020.
[23] J. Sun, A. Li, and K. M. Luk, "A high-gain millimeter-wave magnetoelectric dipole array with packaged microstrip line feed network," *IEEE Antennas and Wireless Propagation Letters*, vol. 19, no. 10, pp. 1669–1673, 2020.
[24] Y. J. Li, C. Wang, and Y. X. Guo, "A Ka-band wideband dual-polarized magnetoelectric dipole antenna array on LTCC," *IEEE Transactions on Antennas and Propagation*, vol. 68, no. 6, pp. 4985–4990, 2020.
[25] Q. L. Yang, S. Gao, L. Wen, *et al.*, "Cavity-backed slot-coupled patch antenna array with dual slant polarization for millimeter-wave base station applications," *IEEE Transactions on Antennas and Propagation*, vol. 69, no. 3, pp. 1404–1413, 2021.
[26] J. Xu, W. Hong, Z. H. Jiang, *et al.*, "Millimeter-wave broadband substrate integrated magneto-electric dipole arrays with corporate low-profile microstrip feeding structures," *IEEE Transactions on Antennas and Propagation*, vol. 68, no. 10, pp. 7056–7067, 2020.
[27] X. Dai and K. M. Luk, "A wideband dual-polarized antenna for millimeter-wave applications," *IEEE Transactions on Antennas and Propagation*, vol. 69, no. 4, pp. 2380–2385, 2021.
[28] J. Xu, W. Hong, Z. H. Jiang, *et al.*, "Low-cost millimeter-wave circularly polarized planar integrated magneto-electric dipole and its arrays with low-profile feeding structures," *IEEE Antennas and Wireless Propagation Letters*, vol. 19, no. 8, pp. 1400–1404, 2020.
[29] C. Y. D. Sim, C. C. Chang, and J. S. Row, "Dual-feed dual-polarized patch antenna with low cross polarization and high isolation," *IEEE Transactions on Antennas and Propagation*, vol. 57, no. 10, pp. 3405–3409, 2009.
[30] W. Wang, J. Wang, A. Liu, *et al.*, "A novel broadband and high-isolation dual-polarized microstrip antenna array based on quasi-substrate integrated waveguide technology," *IEEE Transactions on Antennas and Propagation*, vol. 66, no. 2, pp. 951–956, 2018.
[31] S. S. Yao, Y. J. Cheng, H. Bai, *et al.*, "W-band high-efficiency waveguide slot array antenna with low sidelobe levels based on silicon micromachining technology," *Chinese Journal of Electronics*, vol. 31, no. 4, pp. 665–673, 2022.
[32] J. Yang, M. J. Yin, H. Y Gao, *et al.*, "Design and fabrication of reflective phase shifter for two-dimensional terahertz beam-scanning reflectarray," *Chinese Journal of Electronics*, vol. 31, no. 3, pp. 581–588, 2022.
[33] H. Jiang, Y. Yao, and T. Xiu, "High-gain dual circularly polarized antenna for air-to-ground wireless link," *Chin. J. Electron.*, vol. 31, no. 3, pp. 555–561, 2022.
[34] A. Osseiran, J. F. Monserrat, P. Marsch, *et al.*, *5G Mobile and Wireless Communications Technology*. Cambridge University Press, Cambridge, UK, 2016.
[35] Y. F. Geng, W. W. Wang, X. W. Chen, *et al.*, "The study and design of a miniaturized microstrip balun with a wider bandwidth," *IEEE Antennas and Wireless Propagation Letters*, vol. 15, pp. 1727–1730, 2016.
[36] C. J. Liu and W. Menzel, "Broadband via-free microstrip balun using metamaterial transmission lines," *IEEE Microwave and Wireless Components Letters*, vol. 18, no. 7, pp. 437–439, 2008.
[37] Z. Y. Zhang, Y. X. Guo, L. C. Ong, *et al.*, "A new wide-band planar balun on a single-layer PCB," *IEEE Microwave and Wireless Components Letters*, vol. 15, no. 6, pp. 416–418, 2005.

Yang CHENG received the B.S. degree in electrical engineering from the University of Electronic Science and Technology of China (UESTC), Chengdu, China, in 2019, and he is currently working toward the Ph.D. degree with the University of Electric Science and Technology of China (UESTC), Chengdu, China. His research interests include miniaturized antennas, planar antennas and microwave devices for handset and base station applications. He has published more than 20 journal and conference papers, and also holds several patents. He is serving as a reviewer for *IEEE Transaction on Antennas and Propagation*.
(Email: 18482228792@163.com)

Yuandan DONG received the B.S. and M.S. degrees from the Department of Radio Engineering, Southeast University, Nanjing, China, in 2006 and 2008, respectively, and the Ph.D. degree from the Department of Electrical Engineering, University of California at Los Angeles (UCLA), Los Angeles, CA, USA, in 2012. From September 2008 to June 2012, he was a Graduate Student Researcher with the Microwave Electronics Laboratory, UCLA. From September 2012 to February 2016, he was working as a Senior Engineer with the Research and Development Hardware Department, Qualcomm, San Diego, CA, USA. From February 2016 to December 2017, he was working as a Staff Engineer with Universal Electronics Inc., Santa Ana, CA, USA. Since December 2017, he has been a Full Professor with the University of Electronic Science and Technology of China, Chengdu, China. He has authored or coauthored more than 300 journal articles and conference papers, which receive more than 6000 citations. He has been listed as an Elsevier highly cited researcher. He holds more than 100 patents including six international patents. He and his team have developed multiple RF products including acoustic wave filters, antenna tuners, and antennas, which are very widely shipped and applied in mobile devices. His research interests include the characterization and development of RF and microwave components, antennas, RF frontend modules, circuits, acoustic-wave filters, and metamaterials.
(Email: ydong@uestc.edu.cn)